INTERNATIONAL JOURNAL OF HYDROGEN ENERGY XXX (2018) 1–10

Available online at www.sciencedirect.com

ScienceDirect

journal homepage: www.elsevier.com/locate/he

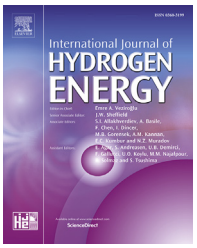

Effect of additive distribution in H_2 absorption and desorption kinetics in MgH_2 milled with $NbH_{0.9}$ or NbF_5

Santiago A. Pighin [a,b,*], *Bruno Coco* [c], *Horacio Troiani* [a,d], *Facundo J. Castro* [a,d], *Guillermina Urretavizcaya* [a,d]

[a] *Consejo Nacional de Investigaciones Científicas y Técnicas (CONICET), Centro Atómico Bariloche, Av. Bustillo, 9500, S.C. de Bariloche, Argentina*

[b] *Centro Regional Universitario Bariloche, Universidad Nacional del Comahue, Quintral, 1250, S.C. de Bariloche, Argentina*

[c] *Facultad de Ingeniería, Universidad Nacional de Cuyo, Centro Universitario, Mendoza, Argentina*

[d] *Instituto Balseiro, Universidad Nacional de Cuyo, Av. Bustillo 9500, S.C. de Bariloche, Argentina*

ARTICLE INFO

Article history:
Received 19 December 2017
Received in revised form
23 February 2018
Accepted 24 February 2018
Available online xxx

Keywords:
Hydrogen storage
Magnesium hydride
Niobium hydride
Niobium fluoride
Hydriding/dehydriding kinetics
Ball milling

ABSTRACT

This paper presents a comparative study of H_2 absorption and desorption in MgH_2 milled with NbF_5 or $NbH_{0.9}$. The addition of NbF_5 or $NbH_{0.9}$ greatly improves hydriding and dehydriding kinetics. After 80 h of milling the mixture of MgH_2 with 7 mol.% of NbF_5 absorbs 60% of its hydrogen capacity at 250 °C in 30 s, whereas the mixture with 7 mol.% of $NbH_{0.9}$ takes up 48%, and MgH_2 milled without additive only absorbs 2%. At the same temperature, hydrogen desorption in the mixture with NbF_5 finishes in 10 min, whereas the mixture with $NbH_{0.9}$ only desorbs 50% of its hydrogen content, and MgH_2 without additive practically does not releases hydrogen. The kinetic improvement is attributed to $NbH_{0.9}$, a phase observed in the hydrogen cycled $MgH_2 + NbF_5$ and $MgH_2 + NbH_{0.9}$ materials, either hydrided or dehydrided. The better kinetic performance of the NbF_5-added material is attributed to the combination of smaller size and enhanced distribution of $NbH_{0.9}$ with more favorable microstructural characteristics. The addition of NbF_5 also produces the formation of $Mg(H_xF_{1-x})_2$ solid solutions that limit the practically achievable hydrogen storage capacity of the material. These undesired effects are discussed.

Introduction

MgH_2 continues to be one of the most promising materials for hydrogen storage due to its high capacity (7.6 wt%), low cost, environmental friendliness and ubiquity (one of the most important Mg reservoirs is sea water). Besides, it has good reversibility during successive cycles of hydrogen absorption and desorption. This is why there is still much research being done to overcome its main drawbacks: its low desorption pressure at operative temperatures and its slow kinetics.

Regarding kinetics, many advances have been achieved by the use of ball milling. This technique, which comminutes MgH_2 particles, reduces crystallite size, and generates defects

* *Corresponding author.*
E-mail address: spighin@cab.cnea.gov.ar (S.A. Pighin).

https://doi.org/10.1016/j.ijhydene.2018.02.151

Please cite this article in press as: Pighin SA, et al., Effect of additive distribution in H_2 absorption and desorption kinetics in MgH_2 milled with $NbH_{0.9}$ or NbF_5, International Journal of Hydrogen Energy (2018), https://doi.org/10.1016/j.ijhydene.2018.02.151

and strain, considerably improves hydrogen absorption and desorption kinetics [1]. An extra benefit is obtained through the use of additives [2]. In particular, Nb-based additives like NbH_x ($x < 1$), Nb and NbF_5 have shown promising results [3–22]. In the case of MgH_2 milled with NbH_x, a physical mixture is formed where morphological and structural properties of both compounds are refined yielding kinetic improvements. For example, Zhang et al. [3] have compared hydrogen sorption kinetics in MgH_2 milled with three kinds of NbH_x-nanoparticles synthesized by wet-chemical methods, and have observed that the better performance is obtained with the additive with more disordered structure and/or smaller particle sizes. Song et al. [4] have studied the behavior of MgH_2 milled with NbH_x obtained by hydriding commercial Nb, and have reported an improvement in hydrogen absorption and desorption kinetics, and a significant decrease in thermal desorption temperature. Regarding Nb as additive, it has been incorporated to MgH_2 or Mg by milling [5–9], by sputtering [10,11] or by hydrogen plasma metal reaction (HPMR) [12]. Huot et al. [5,6] have studied 20 h-ball-milled MgH_2 + 5 at.% Nb and have achieved complete hydrogen desorption in 5 min at 573 K. They have also reported the formation of a metastable NbH_x ($x \approx 0.6$) phase during hydrogen desorption that they suggest could act as a hydrogen gateway. In addition, Pelletier et al. [13] and Kim et al. [14] have suggested that this metastable NbH_x would prevent Mg/MgH_2 coalescence. de Castro et al. [7] have studied the behavior of Mg–Nb nanocomposites processed by reactive milling and have reported a decrease in the thermal desorption temperature of the nanocomposites. For a similar content of Nb, a moderate improvement has been reported by Gasan et al. [8] after only 2 h of milling. Interestingly, core-shell like nanostructures have been prepared by milling and mixing Mg/MgH_2 and $NbCl_5$ in THF by Cui et al. [9]. These materials have presented very good kinetic performance with an important decrease in thermal desorption temperature and considerable dehydriding even at 225 °C. Additionally, Nb nanoclusters and nanoparticles have also shown significant catalytic properties in Mg–Nb films and nanocomposites [10–12]. Concerning NbF_5, Luo et al. [15] have reported better hydrogen sorption kinetics in a mechanically milled MgH_2 + 2 mol.% NbF_5 mixture compared with a MgH_2 + 2 mol.% Nb + 5 mol.% MgF_2 material synthesized under the same conditions. Jin et al. [16,17] have shown very promising results in isothermal absorption kinetics and non-isothermal desorption, with remarkable good behavior of NbF_5 among several transition-metal fluorides. Recham et al. [18] have reported that the addition of NbF_5 produces better hydrogen sorption kinetic behavior than the use of $NbCl_5$ or Nb_2O_5. And Malka et al. [19,20] have studied the effect on hydrogen sorption kinetics of adding different halides to MgH_2 and have reported an excellent performance of NbF_5 over all the studied compounds, only overcame by ZrF_4. Finally, Floriano et al. [21] have shown by DSC and volumetric experiments that the addition of NbF_5 to MgH_2 results in better hydrogen absorption and desorption kinetics than the incorporation of Nb_2O_5 or Nb.

It has been reported that when NbF_5 and MgH_2 are milled together, they react producing NbH_x and MgF_2 [16]. However, further studies using greater NbF_5 amounts have shown that a solid solution $Mg(H_{0.8}F_{0.2})_2$ with H^- partially substituted by F^- is formed [22]. The effect on hydrogen sorption kinetics of these compounds is not clear yet [23–27]. According to some reports, MgF_2 is not beneficial for hydrogen absorption and desorption. For example, Leiva et al. [23] have observed that the onset desorption temperature is slightly higher in MgH_2 obtained by milling Mg + MgF_2 under H_2 than in MgH_2 obtained by milling pure Mg. Similarly, Ma et al. [24] have reported that MgH_2 and MgH_2 + 6 mol.% MgF_2 have comparable absorption and desorption properties. More recently, Tortoza et al. [25] have presented a study of the Mg–H–F system and have shown that hydrogen take up and release in $Mg(H_xF_{1-x})_2$ solutions have slower kinetics than in MgH_2. On the contrary, Jain et al. [26] have shown that MgH_2 + MgF_2 presents better hydriding and dehydriding kinetics than MgH_2 without additive. And, in a different system (MgH_2 + TiF_3), Mulder et al. have proposed that MgF_2 could enhance hydrogen absorption by acting as a nucleation center for MgH_2 [27].

From this literature survey it is clear that the addition of Nb or Nb-based compounds has a substantial effect on hydrogen absorption and desorption kinetics. However, it is interesting to note that the comparison of the effect of different Nb compounds added to MgH_2 in identical proportion following the same experimental procedure has only been made in a few cases [15,21]. In particular, to the best of our knowledge, there are no reports that compare the effects of NbF_5 and NbH. Additionally, there is still disagreement on the effect of MgF_2 on hydrogen sorption kinetics [23–27]. Taking all this into account, we present here the study of hydrogen absorption and desorption behavior of two systems obtained by mechanical milling: MgH_2 + $NbH_{0.9}$ and MgH_2 + NbF_5. By comparing these materials we identify that $NbH_{0.9}$ is the phase that produces the kinetic improvement, and establish some differences among the $NbH_{0.9}$ incorporated as additive and that produced from the reaction between NbF_5 and MgH_2. These differences correlate with the kinetic performance of the materials. Additionally, we discuss the effects of $Mg(H_xF_{1-x})_2$ solid solutions that form instead of MgF_2 during milling. In particular, we analyze their effect on hydrogen sorption and the limitations they impose for hydrogen storage.

Materials and methods

The materials were prepared using commercial MgH_2 (Sigma Aldrich, 96.5%, particle sizes in the 10–100 μm range), NbF_5 (Sigma Aldrich, 98%), and lab-made $NbH_{0.9}$. The Nb hydride was obtained by hydriding small pieces of Nb (Alfa Aesar, 99.95%) at 450 °C and subsequently milling under 5 bar H_2 at room temperature. The Rietveld refinement of the diffractogram confirms that all the peaks correspond to the orthorhombic β-$NbH_{0.9}$ phase (the composition was determined by interpolating composition vs. cell volume data available in the literature [28–31]). Mixtures of MgH_2 + 7 mol.% $NbH_{0.9}$ were milled in a low energy milling device (Uni-Ball-Mill II, Australian Scientific Instruments) for 10 and 80 h with a ball-to-powder mass ratio equal to 50:1 under Ar atmosphere. These materials are labeled MN10 and MN80, respectively. Additionally, a MgH_2 + 7 mol.% NbF_5 mixture was milled under the same conditions of MN80. This material is labeled MNF80. As a reference, commercial MgH_2 was milled under identical conditions (labeled M80).

Please cite this article in press as: Pighin SA, et al., Effect of additive distribution in H_2 absorption and desorption kinetics in MgH_2 milled with $NbH_{0.9}$ or NbF_5, International Journal of Hydrogen Energy (2018), https://doi.org/10.1016/j.ijhydene.2018.02.151

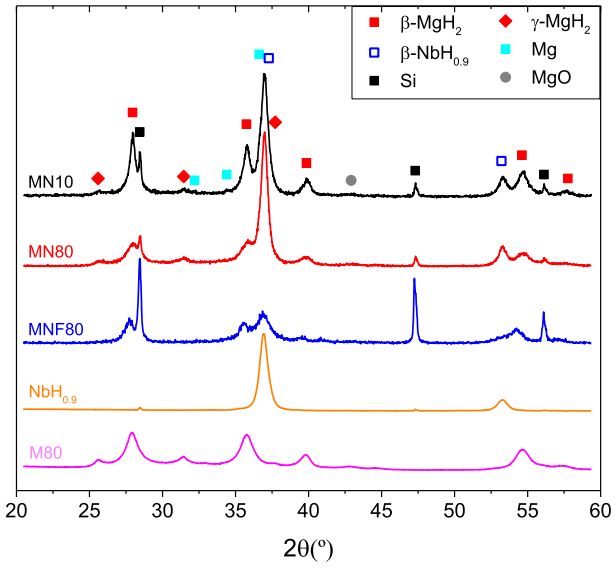

Fig. 1 – X-ray diffractograms of the as-milled materials and the $NbH_{0.9}$ used as additive.

Phase identification and structural characterization was performed by X-Ray powder diffraction (XRD) on a Bruker Advance D8 instrument with Cu Kα radiation. For a precise determination of peak positions, silicon powder was added to the samples as an internal standard. The positions of the diffracted peaks were compared with the ICDD PDF card positions for phase identification. Rietveld refinement was done with TOPAS [32]. Morphology was analyzed by scanning electron microscopy (SEM) and elemental analysis was determined by energy dispersive X-ray spectroscopy (EDS) (SEM FEI Nova Nano 230 and SEM FEI Inspect S50 microscopes). Transmission electron microscopy (TEM) analysis including high-resolution (HR-TEM) was carried out on FEI TECNAI F20 and Philips CM200 microscopes operated at 200 kV. Bright field (BF) and dark field (DF) images were formed after performing selected area electron diffraction (SAED) patterns. Differential scanning calorimetry (DSC) was measured on a Q2000 device (TA Instruments) under 122 ml/min Ar flux and 5 °C/min heating rate from room temperature to 460 °C. Thermogravimetric analysis (TG) was performed on a TGA-HP50 apparatus (TA Instruments) under 50 ml/min He flux with the same temperature setting of the DSC experiments. Hydrogen absorption and desorption at 250 °C was measured at 1000 kPa and 20 kPa, respectively on a custom-made volumetric apparatus [33]. Before the measurements, 3 cycles of desorption and absorption at 300 °C were performed to assure repeatability of the sorption curves. Sample handling was done in an Ar-filled glovebox (UNILab-MBraun, O_2 and H_2 levels below 1 ppm).

Results

Structural and morphological characterization

The diffractograms of the as-milled MN10 and MN80 show peaks that correspond to β-MgH_2 (PDF 00-012-0697), β-$NbH_{0.9}$, γ-MgH_2 (PDF 00-035-1184) and Si (PDF 00-026-1481, internal standard) (Fig. 1). β-MgH_2 and β-$NbH_{0.9}$ are the main phases (see Table 1 with the phase proportions obtained by Rietveld refinement) and they are the expected phases taking into account the starting materials. In particular, the Nb hydride peak positions in MN10 and MN80 coincide with those of the starting β-$NbH_{0.9}$, which means that there are no compositional changes as a consequence of milling. The high pressure γ-MgH_2 phase is typically produced when MgH_2 is milled [34]. There are also traces of Mg (PDF 00-035-0821, MN10 only) and MgO (PDF 00-045-0946) that are undoubtfully identified by Rietveld refinement. Mg is an impurity of commercial MgH_2 and MgO forms by reaction with ambient oxygen during the XRD measurement.

Fig. 1 also shows the diffractogram of MNF80. Besides Si peaks, reflections corresponding to a $Mg(H_{0.8}F_{0.2})_2$ solid solution [22] and β-$NbH_{0.9}$ can be seen. For the latter, the reflection positions coincide with that observed in MN10 and MN80. The formation of these compounds can be explained by the following two reactions taking place during milling. The first one is:

$$5\,MgH_2 + 2\,NbF_5 \rightarrow 5\,MgF_2 + 2\,NbH_{0.9} + 4.1\,H_2, \quad (1)$$

where MgH_2 and NbF_5 yield MgF_2 and $NbH_{0.9}$. Then, MgF_2 and the remaining MgH_2 react to produce a unique solution of stoichiometry $Mg(H_{0.8}F_{0.2})_2$, according to:

$$x\,MgH_2 + (1-x)\,MgF_2 \rightarrow Mg(H_xF_{1-x})_2. \quad (2)$$

This reaction has already been observed in ball-milled MgH_2 + MgF_2 [25,35]. It is also worth to mention, that γ-MgH_2 is not observed in this material due to the action of F that may hinder its formation [22,35].

In Fig. 1 we also see that milling widens β-MgH_2 peaks in M80 and MN80, and $Mg(H_{0.8}F_{0.2})_2$ peaks in MNF80 due to crystallite size reduction, microstrain and defects induced by milling. To compare the microstructure of the materials, we refined the diffractograms considering peak breadth exclusively due to crystallite size and instrument effects. We had to make this simplifying assumption because the presence of compositional inhomogeneity in MNF80 makes impossible to obtain reliable crystallite size and microstrain values.

Table 1 – Phase abundances (wt%) of the as-milled materials and the corresponding refinement quality.

	β-MgH_2	$Mg(H_{0.8}F_{0.2})_2$	β-$NbH_{0.9}$	γ-MgH_2	Mg	δ-NbH_2	MgO	R_{wp} (%)	χ^2
MN10	69	–	17	7	3	–	4	9.1	1.9
MN80	58	–	22	16	–	–	4	8.7	2.1
MNF80	–	77	15	–	–	1	7	9.8	1.3

Please cite this article in press as: Pighin SA, et al., Effect of additive distribution in H_2 absorption and desorption kinetics in MgH_2 milled with $NbH_{0.9}$ or NbF_5, International Journal of Hydrogen Energy (2018), https://doi.org/10.1016/j.ijhydene.2018.02.151

Table 2 – Crystallite sizes of Nb and Mg-containing phases in the as-milled materials and in the materials obtained after desorption in DSC experiment. The quality of the refinement is also showed.

	as-milled material				after desorption in DSC			
	Crystallite size (nm)		Quality		Crystallite size (nm)		Quality	
	β-$NbH_{0.9}$	β-MgH_2/$Mg(H_{0.8}F_{0.2})_2$	R_{wp} (%)	χ^2	Nb	$Mg/Mg(H_{0.3}F_{0.7})_2$	R_{wp} (%)	χ^2
$NbH_{0.9}$	20	–	8.9	2.6	–	–	–	–
M80	–	8	5.2	2.6	–	289	9.2	1.3
MN10	24	15	9.1	1.9	32	169	6.6	2.2
MN80	26	8	8.7	2.1	26	63	6.4	2.0
MNF80	9	11	9.8	1.3	10	43	3.7	1.5

However, as it will be shown below, this approximation gives crystallite sizes in agreement with TEM images. In the refinement, we have included β-MgH_2, γ-MgH_2 and MgO (M80, MN10 and MN80), $Mg(H_xF_{1-x})_2$ and MgO (MNF80); and β-NbH_z, Mg and Si (MN10, MN80 and MNF80). For $Mg(H_xF_{1-x})_2$, we have used a rutile-type $P4_2/mnm$ structure with Mg^{2+} filling Wyckoff position 2*a* and anions H^- and F^- with refinable occupancies x and 1-x respectively at position 4*f*, as suggested by the structure of β-MgH_2 and MgF_2 [22,35]. The results are shown in Table 2. We observe that β-MgH_2 crystallite size is not affected by $NbH_{0.9}$ addition as it shows similar values in M80 and MN80. Moreover, $Mg(H_{0.8}F_{0.2})_2$ in MNF80 also has a comparable crystallite size. Therefore, we conclude that neither $NbH_{0.9}$ nor NbF_5 affect β-MgH_2/$Mg(H_xF_{1-x})_2$ crystallite size during milling. β-MgH_2 crystallite size seems to be mainly affected by milling time, as the grain refinement from 15 to 8 nm between MN10 and MN80 suggests. The β-$NbH_{0.9}$ crystallite size in MN10 and MN80 is in the 24–26 nm range, very close to that of the starting $NbH_{0.9}$, showing that its microstructure does not change when further milled with MgH_2. In the case of β-$NbH_{0.9}$ in MNF80, a crystallite of only 9 nm is registered which highlights that the $NbH_{0.9}$ formed from NbF_5 has better microstructural characteristics.

SEM images show that different distributions of $NbH_{0.9}$ can be obtained depending on the nature of the additive and milling time. In Fig. 2 we show images of the as-milled materials obtained from backscattered electrons. According to EDS, bright particles correspond to $NbH_{0.9}$ and the rest to MgH_2 (grey). MN10 shows an inhomogeneous distribution of $NbH_{0.9}$, comprising a wide range of particle sizes. Fig. 2A shows a few particles of ~20 μm together with particles smaller than 2 μm embedded in the MgH_2 matrix. After 80 h of milling $NbH_{0.9}$ is more homogeneously distributed, no 20 μm particles can be seen and particles of ~2 μm are still recognizable (Fig. 2B). Notably in MNF80 no individual $NbH_{0.9}$ particles can be seen (Fig. 2C). However, EDS analyses performed in different areas of 80 × 80 μm reveals a molar Mg to Nb ratio of 14 and a F to Nb ratio equal to 5, very close to the nominal values 13.3 and 5.0, respectively. Evidently, $NbH_{0.9}$ particles are smaller than SEM resolution in backscattered electron mode. Similar observations were reported by Floriano et al. for MgH_2 cryo-milled with 2 mol.% NbF_5 [21]. Niobium distribution in MNF80 was also studied by TEM. The similar interplanar distance of the β-$NbH_{0.9}$ (011) and MgO (111) planes makes difficult to distinguish between these compounds. For this reason, a dehydrided MNF80 sample containing Nb instead of $NbH_{0.9}$ was analyzed in order to unequivocally differentiate the phases. Fig. 3 shows a high-resolution image where a Nb distribution in the nanoscale range can be appreciated. Nb crystallites in the 5–15 nm range are intermixed with nanometric $Mg(H_{0.3}F_{0.7})_2$ and Mg crystallites. From this image we can infer that crystallites are also individual particles. In addition, EDS analyses performed using a spot of around 150 nm in diameter give a Mg/Nb ratio equal to 14. This microstructure is similar to the one reported by Malka et al. [36], and differs from that described by Kim et al. [14], where a coating of niobium around MgH_2 is mentioned.

Thermal analysis

The effect of the additives in desorption kinetics and H-capacities of MN80 and MNF80 can be observed in the curves from calorimetric and thermogravimetric experiments shown in Fig. 4. MN10, MN80, MNF80 and the reference M80 deliver hydrogen in an endothermic event that correlates with the mass decreases registered in the TG curves. In the case of MN80, the hydrogen desorption onset temperature is 233 °C (DSC), 54 and 105 °C below the value registered for MN10 and M80, respectively. The H content for MN10, MN80 and M80 are 6.1, 6.2 and 7.1 wt%, respectively, very close to the theoretical values 6.3 for MN10 and MN80, and 7.6 wt% for M80. The reaction involved in H_2 desorption from MN10 and MN80 is mainly the decomposition of β and γ-MgH_2. $NbH_{0.9}$ dehydriding (confirmed by the diffractogram of the sample after DSC and TG) that accounts for a theoretical 0.2 wt% H_2 is not observed as an independent peak. In the case of MNF80, we observe that the TG curve presents two desorption regimes. The first one is fast and is correlated with the endothermic peak that starts at 223 °C (DSC). This regime represents an improvement of 115 °C with respect to the onset temperature of M80. The fast regime is followed by a slow one that starts approximately at 284 °C and is still in progress at 445 °C, the maximum temperature reached during the experiment. The slow mass release of this second regime is correlated with a higher base line in the DSC curve. The desorption in both regimes is caused by the release of H_2 from $Mg(H_{0.8}F_{0.2})_2$ producing an H-poorer solution, Mg and H_2. This process can be stated as follows [35]:

$$Mg(H_xF_{1-x})_2 \leftrightarrow \frac{1-x}{1-y}Mg(H_yF_{1-y})_2 + \frac{x-y}{1-y}(Mg + H_2) \quad (3)$$

The existence of two desorption regimes has been attributed to the limited mobility of F^- ions in the solution which

Please cite this article in press as: Pighin SA, et al., Effect of additive distribution in H_2 absorption and desorption kinetics in MgH_2 milled with $NbH_{0.9}$ or NbF_5, International Journal of Hydrogen Energy (2018), https://doi.org/10.1016/j.ijhydene.2018.02.151

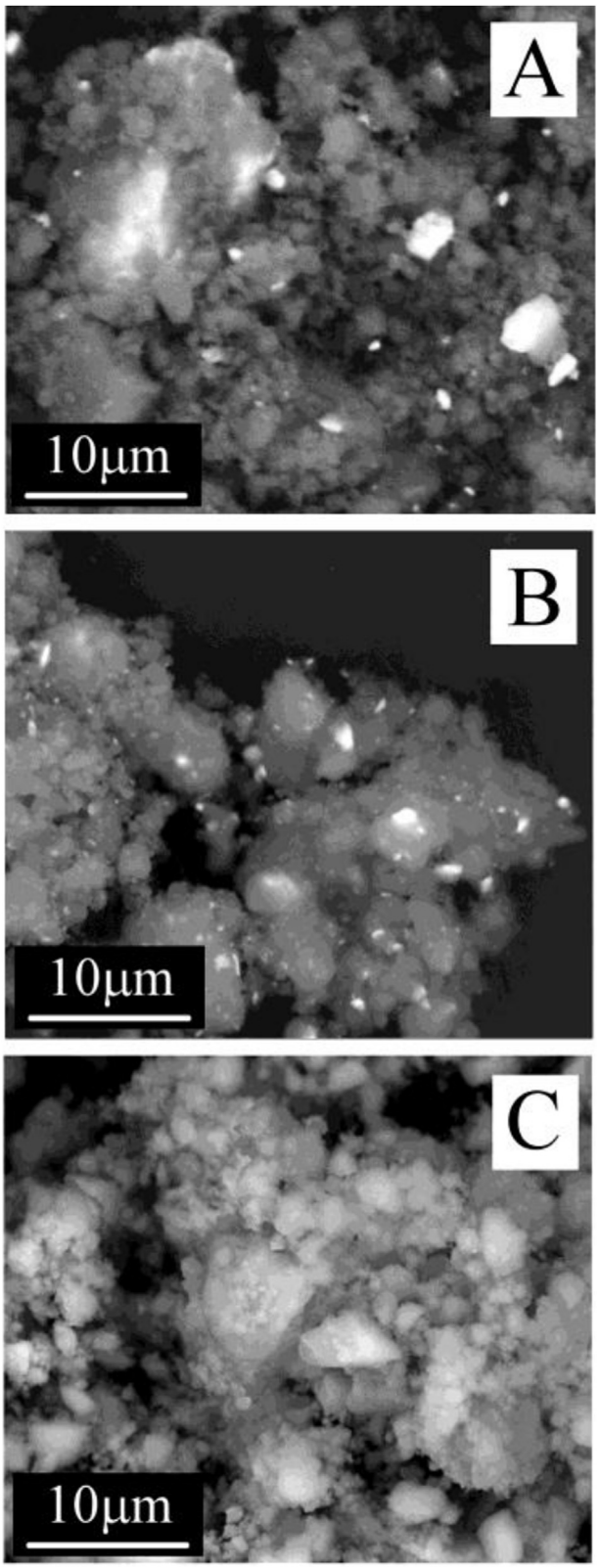

Fig. 2 – Micrographs of the as-milled materials obtained by SEM. MN10 (A), MN80 (B) and MNF80 (C).

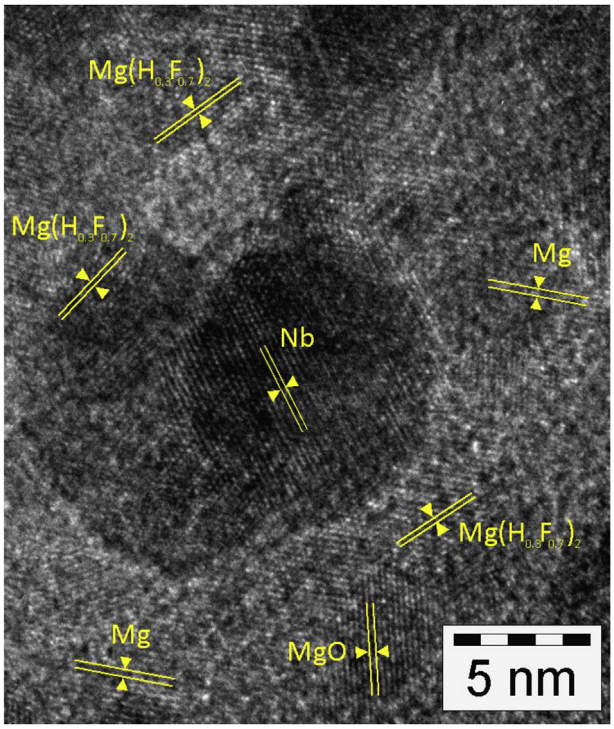

Fig. 3 – HR-TEM image of dehydrided MNF80. The interplanar spacing measured for each phase, and the corresponding family planes are: d = 2.34 Å, Nb{011}; d = 2.46 Å, Mg{011}; d = 2.11 Å, MgO{002}; d = 2.30 Å, $Mg(H_{0.3}F_{0.7})_2${020} and d = 2.06 Å, $Mg(H_{0.3}F_{0.7})_2${210}.

could hinder H^- diffusion when the solution becomes poor in hydrogen [22]. With respect to capacity, the measured value of 3.6 wt% is appreciably lower than the theoretical (4.5 wt%[1]) mainly because of the incomplete desorption at 445 °C. This is confirmed by the diffractograms of the sample after TG and DSC which show peaks that correspond to $Mg(H_{0.3}F_{0.7})_2$.

During DSC and TG experiments there is a recrystallization process activated by temperature that affects the Mg-containing phases. This process is reflected in the increment of the crystallite size as we show in Table 2. M80 exhibits the most marked increase from 8 to 289 nm. In MN10, crystallite grows from 15 to 169 nm, while in MN80 crystallite size increases only from 8 to 63 nm. From these values we deduce that the additive produces an anchoring effect that is more evident when the material is milled longer times. Similarly, MNF80 shows a reduced recrystallization process, exhibiting a crystallite size equal to 43 nm after DSC. This is confirmed by TEM analysis. Fig. 5 shows BF images with SAED patterns and DF images that correspond to the indicated spot. Mg (left) and $Mg(H_{0.3}F_{0.7})_2$ (right) crystallites with size in the range 40–60 nm can be observed. Regarding Nb, crystallite size after thermal desorption is similar to that of β-$NbH_{0.9}$, in accordance with Yavari et al. observations [37].

[1] The lower theoretical capacity of MNF80 respect to MN80 is due to fluorine that substitutes hydrogen in MgH_2 reducing its capacity.

Please cite this article in press as: Pighin SA, et al., Effect of additive distribution in H_2 absorption and desorption kinetics in MgH_2 milled with $NbH_{0.9}$ or NbF_5, International Journal of Hydrogen Energy (2018), https://doi.org/10.1016/j.ijhydene.2018.02.151

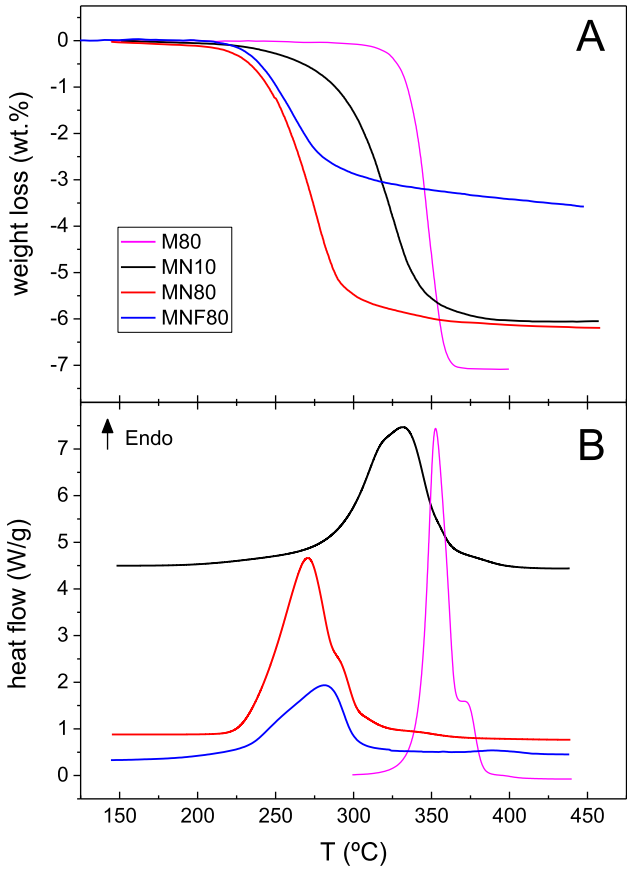

Fig. 4 – TG (A) and DSC (B) curves of M80, MN10, MN80 and MNF80.

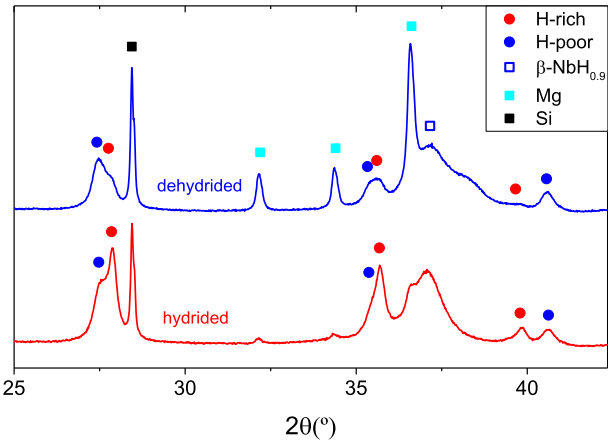

Fig. 6 – X-ray diffractograms of MNF80 after three cycles of desorption-absorption at 300 °C.

Isothermal desorption and absorption of hydrogen

Before comparing hydrogen absorption and desorption in the different materials considered here we want to discuss several aspects of hydrogen absorption and desorption in MNF80. To this end we analyze XRD patterns of hydrided and dehydrided MNF80 acquired after the initial cycles made to ensure repeatability. The most interesting feature in the diffractograms (see Fig. 6) is that both materials present two $Mg(H_xF_{1-x})_2$ solid solutions. In Table 3 we present their details after a Rietveld refinement of the data. One solution is H-rich ($x = 0.81$ and 0.93 for the dehydrided and hydrided material, respectively) and the other is H-poor ($x = 0.34$ and 0.43). The amount of H-poor solid solution shows relatively small changes

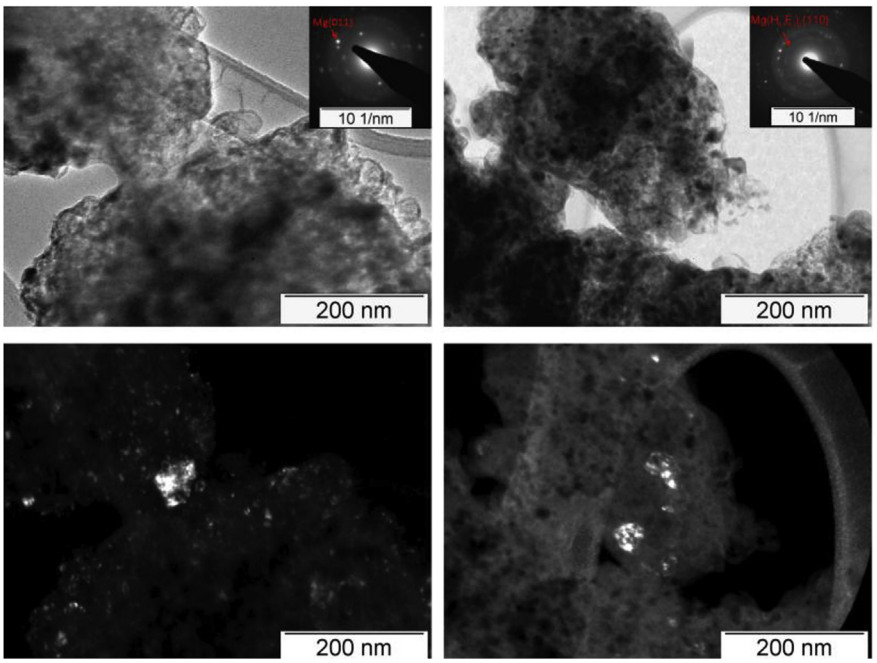

Fig. 5 – BF (upper) and DF (lower) TEM images with SAED (BF inset) of MNF80 dehydrided in DSC. The spots correspond to Mg (left) and $Mg(H_{0.3}F_{0.7})_2$ (right).

Please cite this article in press as: Pighin SA, et al., Effect of additive distribution in H_2 absorption and desorption kinetics in MgH_2 milled with $NbH_{0.9}$ or NbF_5, International Journal of Hydrogen Energy (2018), https://doi.org/10.1016/j.ijhydene.2018.02.151

Table 3 – Rietveld refinement results of hydrided and dehydrided samples after three cycles of desorption-absorption at 300 °C.

MNF80	Solution composition		Abundances (wt.%)						F in H-rich (%)	F in H-poor (%)	Quality	
	$x_{H\text{-}rich}$	$x_{H\text{-}poor}$	H-rich	H-poor	Mg	β-$NbH_{0.9}$	Nb	MgO			$R_{wp(\%)}$	χ^2
dehydrided	0.81	0.34	20	30	28	11	4	7	22	78	4.0	1.8
hydrided	0.93	0.43	39	34	7	14	–	7	20	80	4.3	1.9

between the hydrided and dehydrided material, whereas the quantity of H-rich solution increases considerably in the hydrided material. We can also observe that the F amount in each solid solution before and after desorption is approximately constant, meaning that there is no F–H interchange between the solid solutions. All these features, together with phase abundances and solution compositions are consistent with the following desorption process that considers two simultaneous (3) reactions. In one of these reactions the hydrided H-rich solution (x = 0.93) decomposes into the other H-rich solution with less hydrogen concentration (x = 0.81). This process releases 89% of the total hydrogen desorbed from MNF80 (disregarding the small contribution from the partial dehydriding of $NbH_{0.9}$) and it is the reaction that dominates in hydrogen absorption and desorption experiments. By the other reaction the hydrided H-poor solution (x = 0.43) becomes the other H-poor solution (x = 0.34). This reaction releases the remaining 11% of hydrogen. The composition of the H-poor solutions is around x = 0.4, the value that corresponds to the slow desorption regime in the TG. In this regime the high F concentration limits H-mobility slowing down kinetics [22]. On the other hand, the composition of the H-rich solutions is in the range of the compositions observed during the fast regime in TG experiments. The hydriding process is practically the reverse of the above described process. The H-rich solution takes up hydrogen and gives a solution richer in hydrogen, and the H-poor solution follows a similar process producing a H-poor solution with more hydrogen concentration. The details of these processes are not known yet. One possibility is that H take up occurs by H absorption in a Mg/solid solution interface directly giving a H-richer solution, or, alternatively, it might include two stages, a first one in which Mg takes up H producing MgH_2, and a second one where H diffusion between MgH_2 and a solid solution gives the H-richer solution. The observation of two simultaneous solid solutions somewhat suggests that the second mechanism might take place during hydrogen absorption. If this were the case, considering that for practical reasons the hydriding and dehydriding cycling is carried out in a prefixed time interval, the diffusion process could not reach completion during the absorption time lapse, and therefore two solid solutions instead of a single homogeneous solution would be observed after hydriding. However, to fully establish the mechanism of these processes, further studies are required. Nevertheless, from the practical point of view, hydriding and dehydriding in MNF80 can be considered as the take up and release of hydrogen from the H-rich solid solution.

Comparing now dehydriding performance of all the materials we see that kinetics depends on milling time and the additive used, as can be observed in the desorption curves shown in Fig. 7A. After 10 min, MN10, MN80 and MNF80 complete 10, 50 and 100% of the reaction, respectively, at 250 °C. In contrast, the reference M80 does not significantly dehydride at this temperature, and at 300 °C it releases less than 6% during the same time. The improvement observed comparing MN10 and MN80 can be attributed to milling time, and the substantial reduction of desorption times between MN80 and MNF80 can be linked with the additive distribution and the microstructure of the material, as it will be discussed below. Similar trends are observed during hydrogen absorption (Fig. 7B). MN80 and MNF80 perform considerably better than M80. Additionally, MN80 exhibits better kinetics than MN10, due to the longer milling time, and MNF80 shows slightly fastest kinetics than MN80. After 30 s MN80 completes

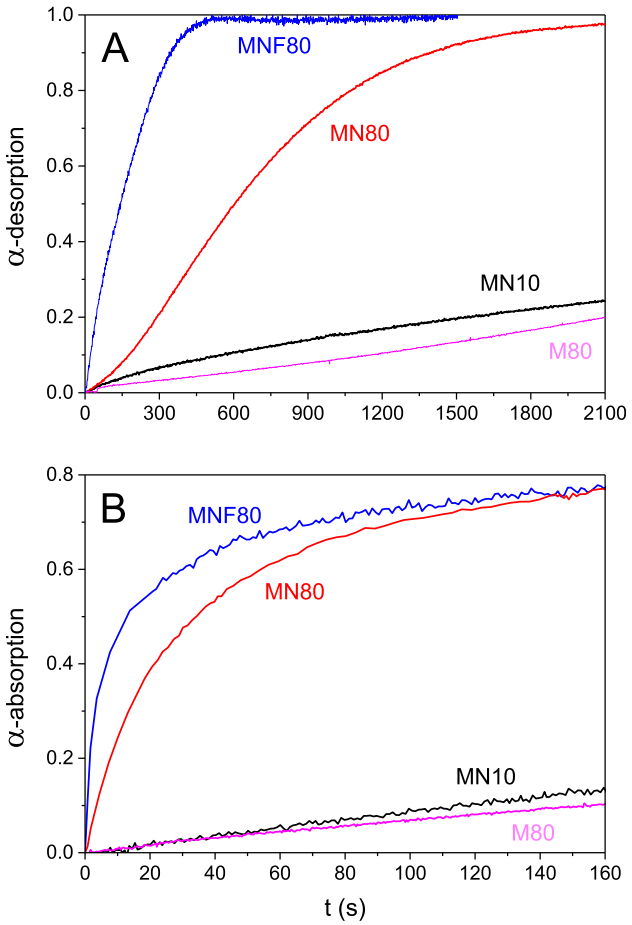

Fig. 7 – Isothermal dehydriding (A) and hydriding (B) curves at 250 °C (unless M80 desorption that was measured at 300 °C).

Please cite this article in press as: Pighin SA, et al., Effect of additive distribution in H_2 absorption and desorption kinetics in MgH_2 milled with $NbH_{0.9}$ or NbF_5, International Journal of Hydrogen Energy (2018), https://doi.org/10.1016/j.ijhydene.2018.02.151

Table 4 – Crystallite sizes of Nb and Mg-containing phases observed in hydrided and dehydrided samples after three cycles of desorption-absorption at 300 °C.

	Dehydrided				Hydrided			
	Crystallite size (nm)		Quality		Crystallite size (nm)		Quality	
	β-$NbH_{0.9}$	Mg	R_{wp} (%)	χ^2	β-$NbH_{0.9}$	β-MgH_2/H-rich	R_{wp} (%)	χ^2
M80	–	198	6.0	2.6	–	136	6.4	2.8
MN10	25	163	6.8	2.9	32	91	8.6	1.2
MN80	29	108	6.0	2.4	28	98	7.7	1.1
MNF80	7	55	4.0	1.8	8	26	4.3	1.9

48% of the reaction whereas MNF80 60%. In all the cases the time needed for absorption is shorter than that for desorption.

Crystallite sizes in the hydrogen-cycled materials are summarized in Table 4. No significant changes in $NbH_{0.9}$ crystallite size are observed between the cycled material and the as-milled material, and between the hydrided and dehydrided material. On the contrary, substantial differences are observed comparing the crystallite sizes of the H-rich solution in MNF80 (26 nm) and MgH_2 in MN80 (98 nm) in the hydrided material, and that of Mg in dehydrided MNF80 (55 nm) and in dehydrided MN80 (108 nm). Recalling also the crystallite sizes of the as-milled materials (Table 2), these results show that grain growth as a consequence of hydrogen cycling is considerably reduced in MNF80 compared with MN80.

Discussion

When Nb-based additives are added to MgH_2 by milling the sorption performance is improved, as we can observe from the lowering of the desorption temperatures in the DSC and TG curves, and from the reduction of the absorption and desorption times in the volumetric experiments. The best results are obtained with MNF80, the material prepared with NbF_5 as additive. The comparison of our results with literature data is summarized in Table 5. It can be seen that the desorption performance of MNF80 exceeds that of the majority of the reported data, with the exception of Jin et al. results [16], that were measured at 300 °C. On the contrary, absorption in MNF80 has an intermediate performance. The materials reported in Refs. [4,6] reach higher conversions after 30 s at 250 °C or even at 200 °C [3], whereas some others [9,12,16] give lower conversions in similar conditions. DSC thermal desorption, typically made on as-milled materials, also presents an average behavior. In Refs. [3,9,17,19] the hydrogen desorption peaks are at lower temperatures, in Refs. [4,15,18] at higher temperatures, and in Ref. [21] at similar temperature. The comparison of MN80 data with literature data shows that this material exhibits intermediate kinetic behavior both in absorption and desorption. Beyond this quantitative comparison, and considering hydriding and dehydriding processes, it is difficult to establish a correlation between the materials characteristics and their hydrogen sorption performance. The tabulated materials were prepared using Nb, NbH_x or NbF_5, in different amounts, employing diverse techniques or milling devices (with different milling times). However, some trends can be found by comparing M80, MN80 and MNF80, as these materials were prepared using the same molar amount of Nb, and following the same procedure. From this comparison we identify several features. First, $NbH_{0.9}$ is the only Nb containing phase that appears in MNF80 and MN80, either hydrided or dehydrided. Second,

Table 5 – Kinetic performance of different MgH_2 + Nb-based additives systems. Isothermal absorption and desorption data are compared using the conversion fraction α, due to the different amount of additive used in each case. Hydriding and dehydriding processes considered at 250 °C, unless explicitly noted in the table. DSC data correspond to as-milled materials measured at a 5 °C/min heating rate, unless explicitly noted in the table.

Ref.	System, preparation technique	Desorption (α after 10 min)	Absorption (α after 30 s)	DSC desorption peak (°C)
3	MgH_2 + 1.5 mol.% NbH_x, milling 2 h	0.86 (270 °C)	0.73 (200 °C)	273
4	MgH_2 + 6.5 mol.% NbH, milling (QM-ISP2) 5 h	–	0.81	322
6	MgH_2 + 5 mol.% Nb, milling (SPEX) 20 h	0.78	0.80	–
9	Mg/MgH_2 + 5 mol.% Nb, mixing in THF	0.48	0.42	244 (4 °C/min)
12	Mg + 2.1 mol.% Nb, HPMR	0.05	0.18	–
15	MgH_2 + 2 mol. % NbF_5, milling (SPEX) 5 h	0.8 (300 °C)	1.0 (300 °C)	364 (cycled material)
16, 17	MgH_2 + 1 mol.% NbF_5, milling (SPEX) 15 min	1.0 (300 °C)	0.46	264
18	MgH_2 + 2 mol.% NbF_5, milling (Retsch) 25 h	0.68	–	360 (10 °C/min)
19	MgH_2 + 1 mol.% NbF_5, milling (P6) 1 h	–	–	262 (cycled material)
21	MgH_2 + 2 mol.% NbF_5, milling (SPEX/cryo) 3 h	0.91 (325 °C)	0.82 (325 °C)	279
MNF80	MgH_2 + NbF_5 7 mol.%, milling (Uni-Ball-Mill II) 80 h	1.0	0.60	280
MN80	MgH_2 + $NbH_{0.9}$ 7 mol.%, milling (Uni-Ball-Mill II) 80 h	0.5	0.48	270

Please cite this article in press as: Pighin SA, et al., Effect of additive distribution in H_2 absorption and desorption kinetics in MgH_2 milled with $NbH_{0.9}$ or NbF_5, International Journal of Hydrogen Energy (2018), https://doi.org/10.1016/j.ijhydene.2018.02.151

$NbH_{0.9}$ particles in MNF80 are substantially smaller and much more dispersed than those of MN80. Third, the crystallite sizes of Mg and $Mg(H_xF_{1-x})_2$ in the hydrogen-cycled MNF80 are considerably smaller than those of Mg and MgH_2 in MN80. And fourth, hydrogen desorption in MNF80 almost doubles that of MN80, whereas hydrogen absorption is slightly better. The substantial differences in hydrogen absorption/desorption in MN80 and MNF80 compared with M80, and the identification of $NbH_{0.9}$ as the sole Nb containing compound in these materials makes us postulate that this phase is the responsible of the observed catalytic effect, in agreement with [3–5,11–14,17]. Comparing now MNF80 and MN80, the observation of an enhanced dispersion of smaller $NbH_{0.9}$ particles when using NbF_5 can be connected with two facts: the low fusion temperature of NbF_5 (76 °C) and the route of $NbH_{0.9}$ formation. It has been suggested [14,16,17,36] that NbF_5 may melt during milling due to local increases of temperature, and the liquid character of the additive may contribute to the enhanced dispersion of $NbH_{0.9}$. In addition, as $NbH_{0.9}$ is formed by reaction (1) during the milling process an intimate mixture with MgH_2 and a good distribution of the additive may be achieved. The smaller size and better distribution of $NbH_{0.9}$, in turn, may play a role in the smaller Mg and $Mg(H_xF_{1-x})_2$/MgH_2 crystallite sizes observed in MNF80. It has been reported [13,14] that $NbH_{0.9}$ particles act as anchors that help keeping small crystallite sizes. The better additive dispersion and microstructure observed in MNF80 has a clear consequence in hydrogen sorption curves. Hydrogen release kinetics in MNF80 almost doubles that of MN80, and hydrogen take up in MNF80 is 25% faster. Smaller and well dispersed $NbH_{0.9}$ particles imply larger Mg/MgH_2-$NbH_{0.9}$ interfaces which contribute to an enhanced $NbH_{0.9}$ catalytic activity.

Concerning a possible catalytic effect of MgF_2 we have observed that $Mg(H_xF_{1-x})_2$ solid solutions are the only F containing compounds observed in the hydrided and dehydrided material. Therefore a MgF_2 catalytic effect does not seem to make sense. Evidently, the small amount of additive typically used in the previous studies has made impossible the identification of these solutions, and therefore its role remains unnoticed. As has been mentioned in Ref. [25], hydrogen take up and release by these solutions are slower than that of Mg/MgH_2, therefore supporting the reports [23,24] that mention that MgF_2 does not improve hydrogen sorption kinetics in Mg/MgH_2. Despite this, hydrogen take up and release in MNF80 presents very good kinetics. Evidently, the strong $NbH_{0.9}$ catalytic effect makes possible to obtain fast hydrogen absorption and desorption in $Mg(H_xF_{1-x})_2$ solutions. However, from the applications point of view, the use of NbF_5 has additional drawbacks. MNF80 has lower capacity than MN80 as has been shown in the TG curves (Fig. 4A). For equal Nb amounts, NbF_5 reduces H_2 storage capacity due to F occupying the same structural sites than H. And additionally, complete hydrogen release from $Mg(H_xF_{1-x})_2$ solutions is practically unachievable due to the slow hydrogen desorption regime of H-poor solutions. Therefore, in the context of the design of Mg-based materials for hydrogen storage, the search of new ways to effectively distribute $NbH_{0.9}$ without the undesired side effects of NbF_5 still remains as an important aspect to improve hydrogen sorption in Mg/MgH_2.

Conclusions

We have shown that NbF_5 or $NbH_{0.9}$ incorporated as additives to MgH_2 by mechanical milling have a significant effect on hydrogen absorption and desorption. Mixtures of MgH_2 and 7 mol.% of NbF_5 can be hydrided at 250 °C up to 60% of its practical hydrogen capacity in 30 s, whereas MgH_2 + 7 mol.% of $NbH_{0.9}$ can take up 48% of hydrogen and MgH_2 milled without additive only absorbs 2% in a similar period. Desorption is also greatly enhanced at 250 °C. The mixture with NbF_5 completely releases its practical hydrogen capacity in 10 min, whereas that with $NbH_{0.9}$ desorbs 50% of its hydrogen content, and MgH_2 without additive practically does not release hydrogen in the same time interval. The kinetic improvement is attributed to the presence of $NbH_{0.9}$, a compound that is present in the cycled materials, either hydrided or dehydrided. Interestingly, $NbH_{0.9}$ particles formed when milling MgH_2 and NbF_5 have substantially smaller sizes and are better distributed than the $NbH_{0.9}$ particles observed when milling MgH_2 and $NbH_{0.9}$. These differences also have a consequence in the smaller Mg and $Mg(H_xF_{1-x})_2$ crystallite sizes observed in the NbF_5 added material. The combination of these advantages gives a material with excellent sorption behavior, compared with other Nb-added materials reported in the literature. However, as hydrogen take up and release occurs in $Mg(H_xF_{1-x})_2$ solid solutions, the practical capacity of the material is limited by the presence of F and the impossibility of completely dehydride the H-poor $Mg(H_xF_{1-x})_2$ solutions. Therefore, further work is needed to synthesize a material with the optimal $NbH_{0.9}$ distribution and microstructure of the NbF_5 added material but without compromising capacity.

Acknowledgements

The authors thank Bernardo Pentke for technical assistance. This work was partially supported by grants from Universidad Nacional de Cuyo (06/C486) and CONICET (PIP 112 201501 00610).

REFERENCES

[1] Huot J, Ravnsbæk DB, Zhang J, Cuevas F, Latroche M, Jensen TR. Mechanochemical synthesis of hydrogen storage materials. Prog Mater Sci 2013;58:30–75. https://doi.org/10.1016/j.pmatsci.2012.07.001.
[2] Webb CJ. A review of catalyst-enhanced magnesium hydride as a hydrogen storage material. J Phys Chem Solids 2015;84:96–106. https://doi.org/10.1016/j.jpcs.2014.06.014.
[3] Zhang L, Xiao X, Xu C, Zheng J, Fan X, Shao J, et al. Remarkably improved hydrogen storage performance of MgH_2 catalyzed by multivalence NbH_x nanoparticles. J Phys Chem C 2015;119:8554–62. https://doi.org/10.1021/acs.jpcc.5b01532.
[4] Song J, Zhao Z, Zhao X, Fu R, Han S. Hydrogen storage properties of MgH_2 co-catalyzed by LaH_3 and NbH. Int J Miner Metall Mater 2017;24:1183–91. https://doi.org/10.1007/s12613-017-1509-z.
[5] Huot J, Pelletier JF, Liang G, Sutton M, Schulz R. Structure of nanocomposite metal hydride. J Alloys Compd

2002;330–332:721–31. https://doi.org/10.1016/S0925-8388(01)01662-0.

[6] Huot J, Pelletier JF, Lurio LB, Sutton M, Schulz R. Investigation of dehydrogenation mechanism of MgH_2-Nb nanocomposites. J Alloys Compd 2003;348:319–24. https://doi.org/10.1016/S0925-8388(02)00839-3.

[7] de Castro JFR, Santos SF, Costa ALM, Yavari AR, Botta WJ, Ishikawa TT. Structural characterization and dehydrogenation behavior of Mg-5 at.% Nb nano-composite processed by reactive milling. J Alloys Compd 2004;376:251–6. https://doi.org/10.1016/j.jallcom.2004.01.021.

[8] Gasan H, Celik ON, Aydinbeyli N, Yaman YM. Effect of V, Nb, Ti and graphite additions on the hydrogen desorption temperature of magnesium hydride. Int J Hydrogen Energy 2012;37:1912–8. https://doi.org/10.1016/j.ijhydene.2011.05.086.

[9] Cui J, Liu J, Wang H, Ouyang L, Sun D, Zhu M, et al. Mg-TM (TM= Ti, Nb, V, Co, Mo or Ni) core-shell like nanostructures: synthesis, hydrogen storage performance and catalytic mechanism. J Mater Chem A 2014;2:9645–55. https://doi.org/10.1039/c4ta00221k.

[10] Bazzanella N, Checchetto R, Miotello A, Sada C, Mazzoldi P, Mengucci P. Hydrogen kinetics in magnesium hydride: on different catalytic effects of niobium. Appl Phys Lett 2006;89:014101. https://doi.org/10.1063/1.2218328.

[11] Mauricio C, Checchetto R, Trapananti A, Rizzo A, D'Acapito F, Miotello A. In situ X-ray absorption spectroscopy – X-ray diffraction investigation of Nb-H nanoclusters in MgH_2 during hydrogen desorption. J Phys Chem C 2015;119. https://doi.org/10.1021/acs.jpcc.5b00252. 77–70.

[12] Liu T, Ma X, Chen C, Xu L, Li X. Catalytic effect of Nb nanoparticles for improving the hydrogen storage properties of Mg-based nanocomposite. J Phys Chem C 2015;119:14029–37. https://doi.org/10.1021/acs.jpcc.5b03442.

[13] Pelletier JF, Huot J, Sutton M, Schulz R, Sandy AR, Lurio LB, et al. Hydrogen desorption mechanism in MgH_2-Nb nanocomposites. Phys Rev B 2001;63:052103. https://doi.org/10.1103/PhysRevB.63.052103.

[14] Kim JW, Ahn J-P, Kim DH, Chung H-S, Shim J-H, Cho YW, et al. In situ transmission electron microscopy study on microstructural changes in NbF_5-doped MgH_2 during dehydrogenation. Scripta Mater 2010;62:701–4. https://doi.org/10.1016/j.scriptamat.2010.01.033.

[15] Luo Y, Wang P, Ma L-P, Cheng H-M. Hydrogen sorption kinetics of MgH_2 catalyzed with NbF_5. J Alloys Compd 2008;453:138–42. https://doi.org/10.1016/j.jallcom.2006.11.113.

[16] Jin S-A, Shim J, Ahn J, Cho Y, Yi K. Improvement in hydrogen sorption kinetics of MgH_2 with Nb hydride catalyst. Acta Mater 2007;55:5073–9. https://doi.org/10.1016/j.actamat.2007.05.029.

[17] Jin S-A, Shim J-H, Cho YW, Yi K-W. Dehydrogenation and hydrogenation characteristics of MgH_2 with transition metal fluorides. J Power Sources 2007;172:859–62. https://doi.org/10.1016/j.jpowsour.2007.04.090.

[18] Recham N, Bhat VV, Kandavel M, Aymard L, Tarascon JM, Rougier A. Reduction of hydrogen desorption temperature of ball-milled MgH_2 by NbF_5 addition. J Alloys Compd 2008;464:377–82. https://doi.org/10.1016/j.jallcom.2007.09.130.

[19] Malka IE, Czujko T, Bystrzycki J. Catalytic effect of halide additives ball milled with magnesium hydride. Int J Hydrogen Energy 2010;35:1706–12. https://doi.org/10.1016/j.ijhydene.2009.12.024.

[20] Malka IE, Pisarek M, Czujko T, Bystrzycki J. A study of the ZrF_4, NbF_5, TaF_5 and $TiCl_3$ influences on the MgH_2 sorption properties. Int J Hydrogen Energy 2011;36:12909–17. https://doi.org/10.1016/j.ijhydene.2011.07.020.

[21] Floriano R, Deledda S, Hauback BC, Leiva DR, Botta WJ. Iron and niobium based additives in magnesium hydride: microstructure and hydrogen storage properties. Int J Hydrogen Energy 2017;42:6810–9. https://doi.org/10.1016/j.ijhydene.2016.11.117.

[22] Pighin SA, Urretavizcaya G, Castro FJ. Study of MgH_2 + NbF_5 mixtures: formation of $MgH_{2-x}F_x$ solid solutions and interaction with hydrogen. Int J Hydrogen Energy 2015;40:4585–96. https://doi.org/10.1016/j.ijhydene.2015.01.153.

[23] Leiva DR, Ishikawa TT, Miraglia S, Fruchart D, Botta WJ. Reactive milling of magnesium under hydrogen using transition metals and their fluorides as additives. Solid State Phenom 2012;194:232–6. https://doi.org/10.4028/www.scientific.net/SSP.194.232.

[24] Ma L-P, Wang P, Cheng H-M. Hydrogen sorption kinetics of MgH_2 catalyzed with titanium compounds. Int J Hydrogen Energy 2010;35:3046–50. https://doi.org/10.1016/j.ijhydene.2009.07.014.

[25] Tortoza MS, Humphries TD, Sheppard DA, Paskevicius M, Rowles MR, Sofianos MV, et al. Thermodynamics and performance of the Mg-H-F system for thermochemical energy storage applications. Phys Chem Chem Phys 2018;20:2274–83. https://doi.org/10.1039/c7cp07433f.

[26] Jain P, Dixit V, Jain A, Srivastava O, Huot J. Effect of magnesium fluoride on hydrogenation properties of magnesium hydride. Energies 2015;8:12546–56. https://doi.org/10.3390/en81112330.

[27] Mulder FM, Singh S, Bolhuis S, Eijt SWH. Extended solubility limits and nanograin refinement in Ti/Zr fluoride-catalyzed MgH_2. J Phys Chem C 2012;116:2001–12. https://doi.org/10.1021/jp204121c.

[28] Manchester FD, editor. Phase diagrams of binary hydrogen alloys. U.S.A: ASM International; 2000. ISBN: 0871705877.

[29] ICDD PDF-2 database release. 2016. cards numbers: 00-039-1327 and 00-007-0263.

[30] Mair G, Bickmann K, Wenzl H. Structural transformation correlated with order-disorder transformations of H in NbH Crystals. Z Phys Chem 1979;114:29–35. https://doi.org/10.1524/zpch.1979.114.114.029.

[31] Cenzual K, Gelato LM, Penzio M, Parthé E. Inorganic structure types with revised space groups. I Acta Cryst 1991;B47:433–9. https://doi.org/10.1107/S0108768191000903.

[32] TOPAS V4: general profile and structure analysis software for powder diffraction data. User's Manual. Karlsruhe: Bruker AXS; 2008.

[33] Meyer G, Rodríguez DS, Castro FJ, Fernández G. Automatic device for precise characterization of hydride forming materials. In: 11th world hydrogen energy conference, vol. 2. Stuttgart: International Association for Hydrogen Energy; 1996. p. 1293.

[34] Gennari FC, Castro FJ, Urretavizcaya G. Hydrogen desorption behavior from magnesium hydrides synthesized by reactive mechanical alloying. J Alloys Compd 2001;321:46–53. https://doi.org/10.1016/S0925-8388(00)01460-2.

[35] Pighin SA, Urretavizcaya G, Castro FJ. Reversible hydrogen storage in $Mg(H_xF_{1-x})_2$ solid solutions. J Alloys Compd 2017;708:108–14. https://doi.org/10.1016/j.jallcom.2017.02.297.

[36] Malka IE, Bystrzycki J, Płociński T, Czujko T. Microstructure and hydrogen storage capacity of magnesium hydride with zirconium and niobium fluoride additives after cyclic loading. J Alloys Compd 2011;509:S616–20. https://doi.org/10.1016/j.jallcom.2010.10.122.

[37] Yavari AR, de Castro JFR, Vaughan G, Heunen G. Structural evolution and metastable phase detection in MgH_2–5%NbH nanocomposite during in-situ H-desorption in a synchrotron beam. J Alloys Compd 2003;353:246–51. https://doi.org/10.1016/S0925-8388(02)01199-4.

Please cite this article in press as: Pighin SA, et al., Effect of additive distribution in H_2 absorption and desorption kinetics in MgH_2 milled with $NbH_{0.9}$ or NbF_5, International Journal of Hydrogen Energy (2018), https://doi.org/10.1016/j.ijhydene.2018.02.151